Membrane resonance in bursting pacemaker neurons of an oscillatory network is correlated with network frequency

Vahid Tohidi

Federated Department of Biological Sciences, Rutgers University

Newark, NJ 07102

Farzan Nadim

Department of Mathematical Sciences, New Jersey Institute of Technology

Federated Department of Biological Sciences, Rutgers University

Newark, NJ 07102

Running Title: Membrane resonance of bursting neurons

Corresponding Author
Farzan Nadim
Department of Mathematical Sciences
New Jersey Institute of Technology
323 Martin Luther King Blvd.
Newark, NJ 07102
farzan@njit.edu
Phone: 973-353-1541
Fax: 973-353-5518

Keywords

Oscillation, central pattern generator, resonance, stomatogastric, computer

ABSTRACT

Network oscillations typically span a limited range of frequency. In pacemaker-driven networks, including many Central Pattern Generators (CPGs), this frequency range is determined by the properties of bursting pacemaker neurons and their synaptic connections; thus, factors that affect the burst frequency of pacemaker neurons should play a role in determining the network frequency. We examine the role of membrane resonance of pacemaker neurons on the network frequency in the crab pyloric CPG. The pyloric oscillations (freq ~1 Hz) are generated by a group of pacemaker neurons: the Anterior Burster (AB) and the Pyloric Dilator (PD). We examine the impedance profiles of the AB and PD neurons in response to sinusoidal current injections with varying frequency and find that both neuron types exhibit membrane resonance, i.e. demonstrate maximal impedance at a given preferred frequency. The membrane resonance frequencies of the AB and PD neurons fall within the range of the pyloric network oscillation frequency. Experiments with pharmacological blockers and computational modeling show that both calcium currents I_{Ca} and the hyperpolarization-activated inward current I_h are important in producing the membrane resonance in these neurons. We then demonstrate that both the membrane resonance frequency of the PD neuron and its supra-threshold bursting frequency can be shifted in the same direction by either DC current injection or by using the dynamic clamp technique to inject artificial conductances for I_h or I_{Ca}. Together, these results suggest that membrane resonance of pacemaker neurons can be strongly correlated with the CPG oscillation frequency.

INTRODUCTION

A variety of neurons in different systems exhibit intrinsic membrane resonance (Gimbarzevsky et al., 1984; Art et al., 1986; Llinas and Yarom, 1986; Puil et al., 1986; Hutcheon et al., 1994), a maximum voltage response to low-amplitude subthreshold oscillatory input currents at a certain preferred (resonant) frequency. Membrane resonance has been associated with low-amplitude subthreshold oscillations of membrane potential (Llinas, 1988; Gutfreund et al., 1995; Lampl and Yarom, 1997; Leung and Yu, 1998) which, in turn, correlates with the probability of action potential generation (Engel et al., 2008). Although the relevance of membrane resonance for field oscillations is relatively well known, few studies have explored a direct relationship between membrane resonance and suprathreshold neuronal activity (but see (Brunel et al., 2003; Richardson et al., 2003; Engel et al., 2008)). Additionally, membrane resonance has been studied primarily in tonically firing neurons that lack intrinsic bursting properties, and thus much less is known about the relevance of membrane resonance in bursting neurons (D'Angelo et al., 2001; Izhikevich et al., 2003).

Central pattern generator networks (CPGs) often involve bursting neurons whose stable oscillatory activity is the basis of rhythmic motor behavior. In many CPGs oscillatory activity arises from the coordinated firing of (conditional) pacemaker neurons that produce bursting activity (Moulins and Cournil, 1982; Hooper and Marder, 1984; Bellingham, 1998). Because bursting oscillations are often associated with low-threshold activated ionic currents, it is possible that these currents may give rise to membrane resonance. If so, the membrane potential resonance properties of these bursting neurons can be potentially correlated with their suprathershold bursting activity and thus contribute to network level oscillations in CPGs.

We examine the role of membrane resonance in the crustacean pyloric network, a well-studied CPG, that is characterized by very stable oscillations (freq ~ 1 Hz) produced by a group of pacemaker neurons. This pacemaker group involves two neuron types, the Anterior Burster (AB) and the Pyloric Dilator (PD), that are strongly electrically coupled and produce synchronized bursting activity. We demonstrate that the pyloric pacemaker

neurons exhibit membrane resonance at a frequency that falls in the range of the network oscillation frequencies. We then explore the ionic mechanisms that underlie the resonance properties of the pacemaker neurons. Finally, we demonstrate that the frequency of membrane resonance of the pacemaker neurons can be correlated with their suprathreshold bursting frequency and therefore the network oscillation frequency. These results suggest that membrane resonance properties of pacemaker neurons can be an important factor in determining the frequency of rhythmic activity in CPGs.

MATERIALS AND METHODS

Experimental protocols

Experiments were carried on adult male crabs (*Cancer borealis*) purchased from local distributors (Newark New Jersey, USA). The animals were maintained in artificial seawater tanks at 12 to 15º C until use. They were anesthetized by cooling on ice for 15-30 minutes prior to dissection. The stomatogastric nervous system (including the STG, the esophageal and paired commissural ganglia) was removed using standard methods (Selverston et al., 1976; Harris-Warrick et al., 1992) and pinned down in a Sylgard-coated Petri dish. The STG was desheathed to expose the cell bodies to intracellular electrodes and to effective superfusion of the neurons using normal saline at 11-13º C, pH 7.4, containing (in mM): 11 KCl, 440 NaCl, 13 $CaCl_2 \cdot 2H_2O$, 26 $MgCl_2 \cdot 6H_2O$, 11.2 Trizma base, 5.1 Maleic acid.

Microelectrodes for neurons impalement were pulled using a Flaming-Brown micropipette puller (P97, Sutter Instruments, CA) and filled with 0.6 M K_2SO_4 + 0.02 M KCL (resistance of 8-12 MΩ for current injection, 15-25 MΩ for recording). Neurons identification was accomplished by matching intracellular action potential recordings to extracellular recordings from identified nerves (Selverston et al., 1976; Harris-Warrick et al., 1992). Intracellular somatic impalements were done with two sharp microelectrodes simultaneously (one for current injection and the other one for recording of voltage response) using Axoclamp 2B amplifiers (Molecular Devices, Foster City, CA) and extracellular recordings were filtered (band-pass 100-5000 Hz) and amplified using a differential AC amplifier model 1700 (A-M systems, Carlsborg, WA).

In experiments measuring the resonance property of neurons the ganglion was superfused with 0.1 µM tetrodotoxin (TTX Biotium, CA). We used 5 to 10 mM Cs^+ for blocking I_h and 12.9 mM Mn^{++} + 0.1 mM Ca^{++} for blocking I_{Ca} (Golowasch and Marder, 1992). Although ZD7288 is as effective for blocking I_h it was not used because Cs^+ is a cleaner blocker in the stomatogastric nervous system and its effect is rapidly reversed (Peck et al., 2006). We used 10 mM TEA (Sigma-Aldrich, MO) and 30 µM Riluzole (Sigma-Aldrich, MO) for blocking potassium currents and persistent sodium current respectively.

Photoinactivation (Miller, 1979) of AB neurons was performed by filling them with the Alexa #568 dye (Invitrogen, CA) and illuminating the STG with a green laser.

Impedance and ZAP current

The ZAP function is a sinusoidal function with fixed amplitude but sweeping frequencies in a given range. The ZAP current can be described as

$$I_{ZAP} = I_{\max} \sin(2\pi f(t) \cdot t)$$

where $f(t)$ produces the range of frequencies that the ZAP function sweeps. In our application, we used an exponential chirp function for $f(t)$ to increase the sampling duration of lower frequencies:

$$f(t) = \frac{f_{\min}}{L}(e^{Lt} - 1) \text{ where } L = \log \frac{f_{\max}}{f_{\min}}.$$

The amplitude of the ZAP current was selected as the minimum amplitude that produced a voltage response within the range of the ongoing PD neuron slow-wave oscillation (around -60 to -33 mV). This amplitude was typically set to 1.5 to 2 nA. In some experiments (when the amplitude was 1.5 nA) a bias DC pulse of less than 0.25 nA was added to the ZAP current to bring the minimum voltage (at lowest frequencies) to -60 mV. We used ZAP current injection to measure the impedance of neurons as a function of the frequency of the injected ZAP current. Impedance contains information about both amplitude and phase of oscillation and is calculated as a function of the input frequency as:

$$Z(f) = \frac{\widetilde{V}(f)}{\widetilde{I}(f)}$$

where $\widetilde{X}$ is the Fourier transform of X (Hutcheon and Yarom, 2000). $Z(f)$ is a complex number; the absolute value of Z is the impedance power and is plotted as a function of frequency. In our results we refer to the impedance power as impedance.

Dynamic clamp

The dynamic clamp technique is used to inject a prescribed artificial conductance corresponding to a specific ionic current into a biological neuron (Goaillard and Marder, 2006). This specific conductance can represent an intrinsic or synaptic current. The dynamic clamp current used was calculated as

$$I_x = \bar{g}_x m_x^p h_x^q (V - E_x)$$

where V is the membrane potential of the neuron recorded in real time, x is the modeled ionic current, m_x is the activation gate, h_x is the inactivation gate, $\bar{g}_x$ is the maximum conductance, E_x is the reversal potential, and p and q are non-negative integers. The activation and inactivation terms are sigmoidal functions of V:

$$\frac{dx}{dt} = \frac{1}{\tau_x}(x_\infty(V) - x)$$
$$x_\infty(V) = \frac{1}{1 + \exp((V - V_x)/k_x)}$$
$$\tau_x = \tau_{x,hi} + (\tau_{x,lo} - \tau_{x,hi})/(1 + \exp((V - V_x)/|k_x|))$$

where $x = m$ or h. Note that the same parameters define the midpoint (V_x) or slope (k_x) of the sigmoidal functions defining x_∞ and τ_x. The sign of k_x determines whether the sigmoidal function is increasing or decreasing as a function of V; thus, the definition of x uses the absolute value of k to ensure that $\tau_x = \tau_{x,lo}$ when $V << V_x$ and $\tau_x = \tau_{x,hi}$ when $V >> V_x$.

The parameters of the currents, $I_{Ca,dyn}$ and $I_{h,dyn}$, used in our dynamic clamp experiments are given in Table 1. When simultaneous dynamic clamp current and constant current injections were required, a Brownlee Precision Amplifier (Santa Clara, CA) was used to add the currents before input to the Axoclamp amplifier.

Data Analysis

Data analysis and measurement of impedance profiles were performed with scripts written in Matlab (Ver 6.5, The MathWorks, Natick, MA). The NI PCI-6070-E board (National

Instruments, Austin, TX) was used for data acquisition and for ZAP current injection with the data acquisition software Scope (Ver 7.71) and DClamp (Ver 1.54). A Digidata 1332A board was utilized for simultaneous data acquisition with the Clampex software. The acquired data were saved as binary files and were analyzed with Readscope (Ver 7.70) and Clampfit. The Clampex and Clampfit software are part of the pClamp package (pClamp 9.2, Molecular Devices, Union City, CA). The Scope, Readscope and Dynamic Clamp software are developed in the Nadim lab and are available freely at (http://stg.rutgers.edu/software/index.htm).

Computational simulations

We used the software Network (Ver 2.07 http://stg.rutgers.edu/software/index.htm) for the simulation of the biophysical model of the PD neuron. This model was based on the two-compartment model of the pacemaker neurons developed by Soto-Treviño et al (2005). A detailed description of the model and its parameters is given in (Soto-Trevino et al., 2005). We modified some parameters so that the membrane resonance frequency was similar to that observed in the biological PD neuron. Because we used the model to compare with recordings done in TTX, the maximal conductances of the fast and persistent sodium currents were set to 0. The only other modified parameters were the following maximal conductances (in μS): g_{CaT} = 2.25, g_{CaS} = 5.4, $g_{K(Ca)}$ = 150 and g_{Kd} =150; and the time constants of I_{CaT} and I_h (in msec): $\tau_{m,CaT} = 1 + 9/(1 + \exp((V + 58)/17))$,

$\tau_{h,CaT} = 80 + 10/(1 + \exp((V + 50)/17))$ and $\tau_{m,h} = 50 + 200/(1 + \exp(-(V + 42.2)/8.73))$.

Statistical analysis

Statistical analysis was performed in SigmaStat (SPSS Inc. San Rafael, CA, USA, Version 2.03) and Origin (OriginLab, Natick, MA, Version 7.02) software packages. Error bars shown indicate SEM. In all statistical tests data were checked for normality. Changes were considered significant if the p value was below $\alpha = 0.05$.

RESULTS

Measurement of membrane resonance in pyloric pacemaker neurons

The pyloric pacemaker neurons, AB and PD, produce stable synchronized bursting oscillations with frequency of around 1 Hz (Nusbaum and Beenhakker, 2002) (Fig. 1A). To examine the impedance profile of the AB and PD neurons, we superfused the preparation with saline containing 10^{-7} M TTX to block all descending modulatory inputs and therefore stop the ongoing oscillations. We then injected a ZAP current input with frequencies sweeping from 0.2 to 3 Hz injected in a time interval of 60 s into either the AB or the PD neuron and measured the impedance $Z(f)$ as a function of frequency (see Materials and Methods). In several experiments (N = 5) we used additional sweeping frequencies from 0.1 to 100 Hz which produced an impedance profile that overlapped with those obtained in the more limited range of 0.2 to 3 Hz and did not produce any additional peaks or troughs. Additionally, changing the direction of the frequency sweep from high to low frequencies did not affect the measured impedance profile.

An example of the voltage response of these neurons to the ZAP current input is shown in Figures 1B1 for the AB neuron and 1B2 for the PD neuron. For both neurons, the impedance profile $Z(f)$ showed a characteristic peak indicating membrane resonance at a preferred frequency (henceforth referred to as Z_{max} and f_{max}). The value of the AB neuron f_{max} was 0.69 ± 0.05 Hz producing Z_{max} values of 23.5 ± 2.3 MΩ (N = 6) and those of the PD neuron were f_{max} = 0.92 ± 0.04 Hz with Z_{max} = 10.1 ± 0.7 MΩ (N = 7). Although, across preparations, there was some variability of the Z_{max} values for either the AB or the PD neuron, the resonance frequency f_{max} was relatively consistent for either neuron. Additionally, both the f_{max} and the Z_{max} values for the AB neuron were significantly different from those of the PD neuron (unpaired Student's *t*-test, p = 0.002 for f_{max} and p < 0.001 for Z_{max}).

In pyloric network, the two PD and AB neurons are electrically coupled; previous studies have demonstrated the dynamics of coupling between these neurons (Rabbah et al., 2005; Soto-Trevino et al., 2005). This studies show the apparent coupling between the AB neuron and the PD neuron is less than 25%; therefore, in case of injection of 1.5 to 2 nA into one

PD neuron, a current with amplitude of less than 0.5 nA might be transmitted to the other PD and the AB neuron. Our experiments with ZAP currents with amplitudes in this range did not lead to any resonance effect (data not shown) presumably because currents in those range did not activate voltage-gated currents involved in producing resonance. We also performed the PD neuron membrane resonance measurement while the second PD neuron was voltage clamped at a holding potential of -60 mV to avoid the activation of its ionic currents. These results showed the f_{max} of the PD neuron is not affected by voltage clamping of the other PD neuron (N = 3). In addition, we measured the membrane resonance property of the PD neuron before and after photo-inactivation of the AB neuron. Our results showed the f_{max} of the PD neuron is independent of the AB neuron membrane resonance properties (N = 3).

The AB neuron is small and very sensitive to impalements. Due to the fact that our measurements with sharp electrodes require impalement of the neuron with two electrodes, we focused on the role of the membrane resonance property of the larger PD neurons and the remainder of the Results section involves only data from PD neurons.

Ionic currents underlying membrane resonance

Previous studies that have examined the underlying ionic mechanisms for membrane resonance have implicated the involvement of a variety of voltage-gated ionic currents including the hyperpolarization-activated inward current I_h (Puil et al., 1994; Strohmann et al., 1994), low-threshold calcium currents I_{Ca} (Hutcheon et al., 1994; Castro-Alamancos et al., 2007), slow non-activating potassium currents (Pape and Driesang, 1998; Castro-Alamancos et al., 2007), the Ca^{2+}-activated K^+ current $I_{K(Ca)}$ (Pape and Driesang, 1998; Vigh et al., 2003) and the persistent sodium current (Wang et al., 2006). We explored the role of various ionic currents on the membrane resonance of the PD neurons using blockers.

Blocking I_h alone (using Cs^+; see Materials and Methods) resulted in an increase of the input impedance of the PD at low frequencies and greatly affected the membrane resonance (Fig. 2A, B). In two out of four experiments, Cs^+ resulted in the disappearance of the

membrane resonance and the lowest frequency (0.15 Hz) produced the largest impedance value; in the other two experiments, Cs^{+} did not obliterate resonance but shifted f_{max} to a much lower frequency (range 0.4 to 0.42 Hz).

Blocking the calcium currents with Mn^{++} had a similar effect on membrane impedance and resonance (Fig. 2A, C). However, in the presence of Mn^{++} the membrane resonance property was abolished in every preparation (N = 4) and the peak impedance was shifted to the lowest frequency (0.15 Hz). Note that blocking I_{Ca} also results in blocking the calcium-dependent potassium current $I_{K(Ca)}$ and therefore these results demonstrate the effects of both currents combined. Additionally, when both I_h and I_{Ca} (and therefore $I_{K(Ca)}$) were blocked, the effect on membrane impedance was very similar to that of blocking I_{Ca} alone (N = 4; not shown).

The fact that two distinct types of voltage-gated ionic currents were crucial for the existence of membrane resonance in the PD neurons was surprising. In order to understand the mechanism by which these currents could both underlie membrane resonance we made use of a previously-published model of the pyloric pacemaker neurons AB and PD (Soto-Trevino et al., 2005; Clewley et al., 2008) and for our purposes we only focused on the model PD neuron. We began by exploring the contribution of various voltage-gated ionic currents in producing membrane resonance. By manipulating or removing different maximal conductances in the model we found that the membrane resonance in these neurons was indeed primarily determined by I_h and I_{Ca}. Manipulating the other ionic currents in the model did not remove the membrane resonance of the model neurons, mainly because most of the model ionic currents are activated at higher voltage thresholds. (However, some ionic currents such as the persistent sodium current and the neuromodulator-activated inward current I_{proc} had some effect on the model resonance amplitude Z_{max} or its frequency f_{max}.) We therefore focused on the roles of the two ionic currents I_h and I_{Ca} (see Materials and Methods). Figure 3 shows the response of this model to a somatic injection of a ZAP current.

As seen in Fig. 3A, blocking I_h in the model changed the shape of the voltage profile in response to the ZAP current, especially at lower frequencies. In particular, the local minimum value observed in the lower envelope of the voltage profile in control disappeared after blocking I_h, resulting in a monotonically-increasing lower envelope (compare dashed curves depicting the lower envelopes in Fig. 3A). We also examined the effect of decreasing or increasing of the I_h current maximum conductances (Figs. 3B and 3C respectively) on the impedance profile of the PD model neuron. These, respectively, had the effect of decreasing or increasing the resonance frequency by changing the impedance levels mainly at lower frequencies, as summarized in Fig. 3D.

Blocking I_h also affected the upper envelope of the voltage profile and shifted the voltage profile to lower voltages, resulting in the possibility that the effects on membrane impedance may be due to this voltage shift (Fig. 4A; compare bars on right). To remove this ambiguity, we injected a depolarizing DC current (0.32 nA DC in addition to the ZAP current) into the model PD neuron so that the upper envelope of the voltage profile after blocking I_h approximately matched that of the control at high frequencies (Fig. 4B; compare bars on the right with Fig. 4A). The resulting voltage profile was similar to that of blocking I_h alone (Fig. 4A): in both cases the membrane resonance shifted to much lower frequencies or was abolished. These simulations indicate that the role of I_h in producing the membrane resonance in our model was primarily due to shaping the lower envelope of the voltage profile in response to a ZAP current input.

In contrast to the effect of blocking I_h, blocking I_{Ca} mainly affected the upper envelope of the voltage profile in response to a ZAP current injection, resulting in the disappearance of the local maximum value in the envelope of the voltage profile (compare dashed curves in Fig. 4C). As a result, the impedance profile after blocking I_{Ca} did not show a resonance peak (Fig. 4E). These results indicate that the main effect of I_{Ca} (in conjunction with $I_{K(Ca)}$) was to shape the upper envelope of the voltage profile.

The effect of blocking both I_h and I_{Ca} in the model neuron is shown in Fig. 4D, indicating that blocking both currents affected both the lower and the upper envelopes of the voltage

profile. Together, these modeling results indicate that I_h and I_{Ca} affect the membrane impedance of the PD neurons by shaping distinct regions of the voltage profile and are therefore both necessary in producing the observed membrane resonance. We note that, in contrast to the model, in the biological PD neuron the effect of I_h and I_{Ca} in shaping the lower and upper envelopes of the voltage profiles in response to a ZAP current injection was not clearly discernible. This may be due to the fact that other ionic currents that contribute to this voltage profile need to be blocked to clearly show this effect.

We also examined the effect of blocking other voltage-gated ionic currents on the impedance profile of the biological PD neurons. In particular, we blocked the high-threshold potassium currents ($I_{K(Ca)}$ and the delayed rectifier current I_{Kd}) by bath application of 10 mM TEA. In these experiments, however, even in the presence of TTX, injection of an external ZAP current often resulted in sporadic and irregular spike-like responses of the membrane potential in response to some cycles of the ZAP input (N = 3; Fig. 5A). These sporadic spikes occurred throughout a range of frequencies during the ZAP current injection (possibly due to the fact that our ZAP function only sweeps a small range of frequencies) and the measurements of input impedance versus frequency were greatly affected by the timing of the sporadic spikes and therefore the results could not be reliably compared with control. When we reduced the maximal conductance of the delayed rectifier and calcium-dependent potassium currents in our model to 20% of the original value, the model PD neurons produced sporadic spikes that were similar in shape and timing to those observed in the biological PD neuron in TEA (Fig. 5B). The model spikes were carried by calcium currents, implying the same for the biological neuron. A complete block of the potassium currents led to calcium spikes throughout the range of the ZAP current injection. We tried reducing the amplitude of the ZAP current to prevent the occurrence of these sporadic spikes (maximum membrane potential was below -40 mV). Not all such sweeps showed a resonance peak. However, in sweeps where it was possible to obtain an impedance profile, there was little difference between the resonance frequency in TEA and control conditions (as in Fig. 5C1 and 5C2).

We used 30 μM Riluzole to block the persistent sodium current (Wu et al., 2005) without bath application of TTX. In these experiments we cut the descending input nerve *stn* to remove the effect of modulatory inputs required for the production of bursting activity in the pyloric pacemaker neurons and examined the response of the PD neuron to a low-amplitude ZAP current that was subthreshold at most frequencies. Injection of such a ZAP current in the control saline produces suprathreshold activity at frequencies near the resonance frequency measured in TTX (not shown). In addition, superfusion of Riluzole did not change the frequency range of suprathreshold activity comparing with superfusion with normal saline or TTX (N = 2).

Resonance and oscillation of the PD neuron

Our results in Fig. 1 indicated that the resonance frequency f_{max} of the pyloric pacemaker neurons AB and PD fall within the range of the frequencies of the ongoing pyloric rhythm. We therefore hypothesized that f_{max} of the PD neurons is correlated with the frequency of bursting oscillation of the pacemaker neurons and therefore the pyloric network frequency. It is a known fact that the oscillation frequency of these pacemaker neurons can be changed by adding a bias DC current (Soto-Trevino et al., 2005). We examined whether adding a bias DC current also shifted the f_{max} of the PD neurons.

An example of the effect of a DC bias current injection in the PD neuron ongoing oscillation is shown in Fig. 6A (Ongoing), demonstrating the known fact that an increase in the DC current amplitude results in faster bursting oscillations. The response of the same PD neurons (after putting the preparation in TTX; Fig. 6A TTX) to a ZAP current injection resulted in a shift of the largest voltage response (arrowheads) which occurs at the membrane resonance frequency f_{max}. When f_{max} was plotted against the PD neuron oscillation frequency $f_{pyloric}$ (using the same value of injected DC current: range -1 to +1.5 nA) before and application of TTX, there was a positive linear correlation between these two factors (Fig. 6B; $R^2 = 0.79 \pm 0.12$, $p < 0.0001$, N = 7 experiments, 2-4 data points per experiment). This correlation indicates that changes in the PD neuron f_{max} can be used as a predictive factor for changes in the ongoing oscillation frequency.

This correlation motivated us to examine whether shifting f_{max} could result in a corresponding shift in the ongoing PD neuron oscillation frequency, thus showing the possibility of a causal relationship. In order to shift f_{max}, we made use of the fact that the membrane resonance of the PD neurons is dependent on two distinct ionic currents, I_h and I_{Ca} (Figs. 2-4). We used the dynamic clamp technique to modify the extent of either of these two currents in the PD neuron by adding (or subtracting) a dynamic clamp version of the current with a positive (or negative) maximal conductance (Bartos et al., 1999; Beenhakker et al., 2005). The implementation of an ionic current with a negative maximal conductance using dynamic clamp is equivalent to reducing the expression of that specific ionic current in the biological neuron.

We tuned the parameters of the model I_h and I_{Ca} currents (used in Figs. 3 and 4) so that adding either current into the PD neuron (in TTX) with dynamic clamp produced a shift in the value of f_{max} in the biological neurons (see Table 1 for parameter values). We then performed a separate set of experiments to examine the effect of adding such a dynamic clamp current on a) the ongoing frequency $f_{pyloric}$ in control saline and b) the PD neuron membrane resonance frequency f_{max} in TTX saline. We found that adding either I_h or I_{Ca} with dynamic clamp resulted in a faster PD neuron oscillation (i.e. shift of $f_{pyloric}$ to higher values) whereas adding a negative-conductance current slowed down the oscillation (Fig. 7A and B). After putting the preparation in TTX, the same dynamic-clamp manipulation resulted in a shift of f_{max} in the same direction. To examine whether the change in $f_{pyloric}$ was correlated with the change in f_{max}, we normalized the changes in either variable to the control value to reduce the variability and performed a linear regression analysis. These results showed a positive correlation between these two frequencies (Fig. 7C; $R^2 = 0.57 \pm 0.088$, $p = 0.001$, $N = 5$ experiments; 2-6 negative and 2-6 positive conductance values done in each experiment). The average shifts of f_{max} and $f_{pyloric}$ are marked by the red and blue points in Fig. 7C.

DISCUSSION

Neuronal bursting activity underlies the generation of network oscillations in many systems. Bursting neurons often have a wide variety of voltage-gated and calcium-dependent ionic currents, many of which have activation thresholds at membrane potentials well below the spike threshold. Due to the complex interaction among the nonlinear ionic currents, it is often difficult to elucidate the factors responsible for the oscillation frequency. In this study we used the concept of membrane resonance, which has been widely used in the analysis of the subthreshold oscillations in spiking neurons, to examine the frequency setting in bursting neurons of the crab pyloric central pattern generator. The characteristics of resonance behavior of neurons capture their essential oscillatory properties within network activity near a preferred frequency (Hutcheon and Yarom, 2000). Therefore, we examined how membrane resonance properties of the neurons in the pyloric pacemaker ensemble may be correlated with the bursting cycle frequency of these neurons.

The pyloric network is a pacemaker-driven neural network with a stable rhythmic activity. In this study we provided three sets of results. First, we showed that the PD and AB neurons, which comprise the pyloric pacemaker ensemble, display membrane resonance and that their maximum impedance frequency (f_{max}) is within the range of the pyloric network oscillation frequency. We then focused on the PD neurons and showed that, in these neurons, membrane resonance is dependent on two distinct types of voltage gated current: the hyperpolarization-activated inward current I_h and the calcium current I_{Ca}. Using simulations of a computational model of the PD neuron previously developed in our lab, we find that I_h and I_{Ca} respectively shape the lower and upper envelopes of the voltage response to the ZAP current, thus contributing to different aspects of the voltage response that produces resonance. Finally, we showed that the membrane resonance frequency of the PD neurons is correlated with their bursting cycle frequency: factors that shift the f_{max} of the PD neuron, such as DC current injection and manipulations of the conductance of I_h and I_{Ca} with dynamic clamp, also change the frequency of the ongoing pyloric oscillations in the same direction.

Resonance and oscillations

Few studies have examined the role of membrane resonance in bursting neurons. One exception has been thalamic neurons. The thalamus is composed of a conglomerate of nuclei involving neurons with significantly different properties and is believed by many researchers to be the pacemaker network for spindle rhythms during sleep (Huguenard, 1998). Neurons of the medial geniculate nucleus, for example, demonstrate a resonance peak at 1 Hz which is influenced by a T-type Ca current (Tennigkeit et al., 1997).

Many oscillatory neurons have been shown to have membrane resonance properties that are correlated with the network oscillatory activity. Inferior olive neurons show an impedance peak between 3 and 10 Hz, which corresponds to the frequency of the spontaneous oscillations in these neurons (Lampl and Yarom, 1997). Additionally, it has been shown that bursting activity and resonance frequency in cerebellar granule cells occur within the theta-frequency range (D'Angelo et al., 2001). Guinea pig frontal cortex neurons show membrane resonance in the range of 3 to 15 Hz based on the level of depolarization. These neurons generate subthreshold oscillations at these frequencies and preferentially respond to inputs arriving at similar frequencies (Gutfreund et al., 1995). Mesencephalic trigeminal neurons also show rhythmic bursting activity as well as membrane resonance (Enomoto et al., 2007). Moreover, several studies have claimed that the basis of the theta rhythm in the hippocampus can be attributed to the membrane resonance frequency of CA1 pyramidal neurons (Hu et al., 2002; Peters et al., 2005; Wang et al., 2006; Giocomo et al., 2007).

Ionic currents underlying resonance

It has been proposed that any ionic current that oppose changes in the membrane voltage and has a slow time constant can contribute to the resonance property (Hutcheon and Yarom, 2000). A variety of ionic currents such as I_h, low-threshold I_{Ca}, slow non-activating potassium currents I_M, the calcium-activated potassium current $I_{K(Ca)}$ and the persistent sodium current I_{NaP}, have been shown to contribute to membrane resonance in different neurons (Puil et al., 1994; Pape and Driesang, 1998; Vigh et al., 2003; Wang et al., 2006; Castro-Alamancos et al., 2007). Many such ionic currents (I_h, I_{NaP}, I_{Ca} and I_M) also contribute to pacemaker activities (Del Negro et al., 2005; Forti et al., 2006; Peck et al., 2006; Tazerart et al., 2008). Layer V cortical pyramidal neurons have been shown to have

resonance at low frequencies and somatic and dendritic I_h has been shown to be the main ionic current underlying resonance behavior in these neurons (Ulrich, 2002). In the PD neuron, the main currents contributing to membrane resonance appear to be I_h, I_{Ca} and $I_{K(Ca)}$, although we have not completely ruled out the indirect influence of other voltage-gated currents. Blocking potassium currents with TEA or reducing $I_{K(Ca)}$ in the model led to sporadic (putative) calcium spikes which interfered with impedance measurements. Because there is no way for blocking the calcium currents without also removing $I_{K(Ca)}$, it is not easy to tease apart the roles of I_{Ca} and $I_{K(Ca)}$ in producing resonance. Theoretical studies have shown that autorhythmicity can be produced by any mechanism that produces membrane resonance at a preferred frequency (Holden, 1980). As such, low-threshold calcium currents may be an essential contributor to the production of oscillations or determining the oscillation frequency in the pyloric pacemaker neurons. Few studies have explored the dynamics of calcium currents in stomatogastric neurons (Hurley and Graubard, 1998; Johnson et al., 2003) and their role in rhythmogenesis in this network remains to be explored.

Resonance and network effects

Some modeling studies have indicated that networks of neurons can demonstrate resonance properties that depend on short-term plasticity of synaptic inputs (Houweling et al., 2002; Maex and De Schutter, 2005). However, in experimental studies, alteration of network frequency by means of manipulation of its synaptic properties has not been reported. It has been shown that short-term plasticity in synapses can produce a maximal synaptic response at a preferred frequency, a property that could be called synaptic resonance (Izhikevich et al., 2003; Drover et al., 2007). In a previous study, we examined the interaction between membrane and synaptic resonance. We showed that a neuron with resonance properties that receives input from a synapse that also shows resonance would have a maximal response at a frequency that lies between the two resonance frequencies. In the current study, synaptic effects were absent in the measurements of the membrane resonance properties because these measurements were done in TTX which blocks all activity, including activity of neurons presynaptic to the PD neuron. As such, the role of synaptic resonance properties on

the oscillatory activity of CPG networks in general and the pyloric network in particular remains to be explored.

A correlation between the resonance frequency of the pacemaker neurons and the bursting oscillation frequency suggests that membrane resonance could be an important factor in setting the frequency of pacemaker-driven networks. However, in large multilayer networks, the influence of the membrane resonance of the pacemaker neurons could be quite different. Modeling simulations of such multilayer networks have shown that the entrainment frequency window by pacemaker neurons decreases exponentially with depth and therefore only small networks can show frequency locking to the pacemaker neurons (Kori and Mikhailov, 2004). Yet, studies in other systems have also indicated that membrane resonance can be related to the network oscillation frequency. The onset of whisking in newborn and young rats, for example, has been shown to be coincident with the expression of I_h and appearance of subthreshold membrane resonance in rat vibrissa motoneurons (Nguyen et al., 2004). Experiments on layer V pyramidal neurons of the cortex have also underlined the band-pass filtering property of these neurons especially at the dendritic level (Ulrich, 2002). Interestingly, a modeling study shows that networks that include different neuronal subtypes, some with resonance properties and others with integrating properties, can produce network stability or flexible responsiveness to external stimuli, depending on the structure of the input spike trains (Muresan and Savin, 2007).

While most studies have focused on the role of membrane resonance in the selectivity of response to inputs at certain frequencies, our findings underline the role of membrane resonance in determining the oscillation frequency of the whole network. In particular, our findings underline the role of the resonance frequency of the pacemaker neurons in determining the oscillation frequency of all follower neurons. Additionally, the pyloric pacemaker neurons also receive synaptic input from follower pyloric neurons at the same frequency. It is therefore possible that in these pacemaker neurons, the membrane resonance property acts both to set the intrinsic bursting frequency and to act as an enhancing mechanism for the synaptic inputs that arrive at this frequency. We also predict that extrinsic and neuromodulatory factors that change I_h or I_{Ca} (Johnson et al., 2003; Peck

et al., 2006) or affect the way these currents interact with other membrane or synaptic properties may change the membrane resonance frequency or the impedance profile and consequently change the oscillation frequency of these neurons.

ACKNOWLEDGMENTS

We thank Jorge Golowasch and Hua-an Tseng for the useful discussions and comments on the manuscript. Supported by NIH MH-60605 (FN).

REFERENCES

Art JJ, Crawford AC, Fettiplace R (1986) Electrical resonance and membrane currents in turtle cochlear hair cells. Hear Res 22:31-36.

Bartos M, Manor Y, Nadim F, Marder E, Nusbaum MP (1999) Coordination of fast and slow rhythmic neuronal circuits. J Neurosci 19:6650-6660.

Beenhakker MP, DeLong ND, Saideman SR, Nadim F, Nusbaum MP (2005) Proprioceptor regulation of motor circuit activity by presynaptic inhibition of a modulatory projection neuron. J Neurosci 25:8794-8806.

Bellingham MC (1998) Driving respiration: the respiratory central pattern generator. Clin Exp Pharmacol Physiol 25:847-856.

Brunel N, Hakim V, Richardson MJ (2003) Firing-rate resonance in a generalized integrate-and-fire neuron with subthreshold resonance. Phys Rev E Stat Nonlin Soft Matter Phys 67:051916.

Castro-Alamancos MA, Rigas P, Tawara-Hirata Y (2007) Resonance (approximately 10 Hz) of excitatory networks in motor cortex: effects of voltage-dependent ion channel blockers. J Physiol 578:173-191.

Clewley R, Soto-Trevino C, Nadim F (2008) Dominant ionic mechanisms explored in spiking and bursting using local low-dimensional reductions of a biophysically realistic model neuron. J Comput Neurosci.

D'Angelo E, Nieus T, Maffei A, Armano S, Rossi P, Taglietti V, Fontana A, Naldi G (2001) Theta-frequency bursting and resonance in cerebellar granule cells: experimental evidence and modeling of a slow k+-dependent mechanism. J Neurosci 21:759-770.

Del Negro CA, Morgado-Valle C, Hayes JA, Mackay DD, Pace RW, Crowder EA, Feldman JL (2005) Sodium and calcium current-mediated pacemaker neurons and respiratory rhythm generation. J Neurosci 25:446-453.

Drover JD, Tohidi V, Bose A, Nadim F (2007) Combining synaptic and cellular resonance in a feed-forward neuronal network. Neurocomputing 70:2041-2045.

Engel TA, Schimansky-Geier L, Herz AV, Schreiber S, Erchova I (2008) Subthreshold membrane-potential resonances shape spike-train patterns in the entorhinal cortex. J Neurophysiol 100:1576-1589.

Enomoto A, Han JM, Hsiao CF, Chandler SH (2007) Sodium currents in mesencephalic trigeminal neurons from Nav1.6 null mice. J Neurophysiol 98:710-719.

Forti L, Cesana E, Mapelli J, D'Angelo E (2006) Ionic mechanisms of autorhythmic firing in rat cerebellar Golgi cells. J Physiol 574:711-729.

Gimbarzevsky B, Miura RM, Puil E (1984) Impedance profiles of peripheral and central neurons. Can J Physiol Pharmacol 62:460-462.

Giocomo LM, Zilli EA, Fransen E, Hasselmo ME (2007) Temporal frequency of subthreshold oscillations scales with entorhinal grid cell field spacing. Science 315:1719-1722.

Goaillard JM, Marder E (2006) Dynamic clamp analyses of cardiac, endocrine, and neural function. Physiology (Bethesda) 21:197-207.

Golowasch J, Marder E (1992) Proctolin activates an inward current whose voltage dependence is modified by extracellular Ca2+. J Neurosci 12:810-817.

Gutfreund Y, Yarom Y, Segev I (1995) Subthreshold oscillations and resonant frequency in guinea-pig cortical neurons: physiology and modelling. J Physiol 483 (Pt 3):621-640.

Harris-Warrick RM, Marder E, Selverston AI, Moulins M (1992) Dynamic Biological Networks: The Stomatogastric Nervous System. Cambridge, MA: MIT Press.

Holden AV (1980) Autorhythmicity and entrainment in excitable membranes. Biol Cybern 38:1-8.

Hooper SL, Marder E (1984) Modulation of a central pattern generator by two neuropeptides, proctolin and FMRFamide. Brain Res 305:186-191.

Houweling AR, Bazhenov M, Timofeev I, Grenier F, Steriade M, Sejnowski TJ (2002) Frequency-selective augmenting responses by short-term synaptic depression in cat neocortex. J Physiol 542:599-617.

Hu H, Vervaeke K, Storm JF (2002) Two forms of electrical resonance at theta frequencies, generated by M-current, h-current and persistent Na+ current in rat hippocampal pyramidal cells. J Physiol 545:783-805.

Huguenard JR (1998) Anatomical and physiological considerations in thalamic rhythm generation. J Sleep Res 7 Suppl 1:24-29.

Hurley LM, Graubard K (1998) Pharmacologically and functionally distinct calcium currents of stomatogastric neurons. J Neurophysiol 79:2070-2081.

Hutcheon B, Yarom Y (2000) Resonance, oscillation and the intrinsic frequency preferences of neurons. Trends Neurosci 23:216-222.

Hutcheon B, Miura RM, Yarom Y, Puil E (1994) Low-threshold calcium current and resonance in thalamic neurons: a model of frequency preference. J Neurophysiol 71:583-594.

Izhikevich EM, Desai NS, Walcott EC, Hoppensteadt FC (2003) Bursts as a unit of neural information: selective communication via resonance. Trends Neurosci 26:161-167.

Johnson BR, Kloppenburg P, Harris-Warrick RM (2003) Dopamine modulation of calcium currents in pyloric neurons of the lobster stomatogastric ganglion. J Neurophysiol 90:631-643.

Kori H, Mikhailov AS (2004) Entrainment of randomly coupled oscillator networks by a pacemaker. Phys Rev Lett 93:254101.

Lampl I, Yarom Y (1997) Subthreshold oscillations and resonant behavior: two manifestations of the same mechanism. Neuroscience 78:325-341.

Leung LS, Yu HW (1998) Theta-frequency resonance in hippocampal CA1 neurons in vitro demonstrated by sinusoidal current injection. J Neurophysiol 79:1592-1596.

Llinas R, Yarom Y (1986) Oscillatory properties of guinea-pig inferior olivary neurones and their pharmacological modulation: an in vitro study. J Physiol 376:163-182.

Llinas RR (1988) The intrinsic electrophysiological properties of mammalian neurons: insights into central nervous system function. Science 242:1654-1664.

Maex R, De Schutter E (2005) Oscillations in the cerebellar cortex: a prediction of their frequency bands. Prog Brain Res 148:181-188.

Miller J, Selverston, AI. (1979) Rapid killing of single neurons by irradiation of intracellularly injected dye. Science 206:702-704.

Moulins M, Cournil I (1982) All-or-none control of the bursting properties of the pacemaker neurons of the lobster pyloric pattern generator. J Neurobiol 13:447-458.

Muresan RC, Savin C (2007) Resonance or integration? Self-sustained dynamics and excitability of neural microcircuits. J Neurophysiol 97:1911-1930.
Nguyen QT, Wessel R, Kleinfeld D (2004) Developmental regulation of active and passive membrane properties in rat vibrissa motoneurones. J Physiol 556:203-219.
Nusbaum MP, Beenhakker MP (2002) A small-systems approach to motor pattern generation. Nature 417:343-350.
Pape HC, Driesang RB (1998) Ionic mechanisms of intrinsic oscillations in neurons of the basolateral amygdaloid complex. J Neurophysiol 79:217-226.
Peck JH, Gaier E, Stevens E, Repicky S, Harris-Warrick RM (2006) Amine modulation of Ih in a small neural network. J Neurophysiol 96:2931-2940.
Peters HC, Hu H, Pongs O, Storm JF, Isbrandt D (2005) Conditional transgenic suppression of M channels in mouse brain reveals functions in neuronal excitability, resonance and behavior. Nat Neurosci 8:51-60.
Puil E, Gimbarzevsky B, Miura RM (1986) Quantification of membrane properties of trigeminal root ganglion neurons in guinea pigs. J Neurophysiol 55:995-1016.
Puil E, Meiri H, Yarom Y (1994) Resonant behavior and frequency preferences of thalamic neurons. J Neurophysiol 71:575-582.
Rabbah P, Golowasch J, Nadim F (2005) Effect of electrical coupling on ionic current and synaptic potential measurements. J Neurophysiol 94:519-530.
Richardson MJ, Brunel N, Hakim V (2003) From subthreshold to firing-rate resonance. J Neurophysiol 89:2538-2554.
Selverston AI, Russell DF, Miller JP (1976) The stomatogastric nervous system: structure and function of a small neural network. Prog Neurobiol 7:215-290.
Soto-Trevino C, Rabbah P, Marder E, Nadim F (2005) Computational model of electrically coupled, intrinsically distinct pacemaker neurons. J Neurophysiol 94:590-604.
Strohmann B, Schwarz DW, Puil E (1994) Subthreshold frequency selectivity in avian auditory thalamus. J Neurophysiol 71:1361-1372.
Tazerart S, Vinay L, Brocard F (2008) The persistent sodium current generates pacemaker activities in the central pattern generator for locomotion and regulates the locomotor rhythm. J Neurosci 28:8577-8589.
Tennigkeit F, Ries CR, Schwarz DW, Puil E (1997) Isoflurane attenuates resonant responses of auditory thalamic neurons. J Neurophysiol 78:591-596.
Ulrich D (2002) Dendritic resonance in rat neocortical pyramidal cells. J Neurophysiol 87:2753-2759.
Vigh J, Solessio E, Morgans CW, Lasater EM (2003) Ionic mechanisms mediating oscillatory membrane potentials in wide-field retinal amacrine cells. J Neurophysiol 90:431-443.
Wang WT, Wan YH, Zhu JL, Lei GS, Wang YY, Zhang P, Hu SJ (2006) Theta-frequency membrane resonance and its ionic mechanisms in rat subicular pyramidal neurons. Neuroscience 140:45-55.
Wu N, Enomoto A, Tanaka S, Hsiao CF, Nykamp DQ, Izhikevich E, Chandler SH (2005) Persistent sodium currents in mesencephalic V neurons participate in burst generation and control of membrane excitability. J Neurophysiol 93:2710-2722.

FIGURE LEGENDS

Figure 1: Membrane resonance measurement of the pyloric pacemaker neurons, AB and PD. Simultaneous recordings of the AB (**A1**) and PD (**A2**) neuron oscillations during the ongoing pyloric rhythm. **B1.** The voltage response of the AB neuron to a 60-second ZAP current injection (top trace) that sweeps a frequency range between 0.1 and 4 Hz indicates a maximum amplitude at a preferred resonance frequency (f_{max}: indicated by arrowhead). **B2.** The voltage trace of the PD neuron in response to a similar ZAP current also shows a resonance frequency f_{max} (arrowhead). The small horizontal dashed lines in A and B show the -50 mV level. **C1.** The impedance profile of the AB neuron in the frequency domain. The cross bar shows the resonance frequency and the maximum impedance value (f_{max} = 0.69 ± 0.05 Hz, Z_{max} = 23.5 ± 2.3 MΩ; N = 6). The shaded region indicates one standard error. **C2.** The impedance profile of the PD neuron (f_{max} = 0.92 ± 0.04, Z_{max} = 10.1 ± 0.7 MΩ; N = 7). Note that the f_{max} and Z_{max} values shown in C1 and C2 do not exactly match the peak of the mean impedance profile (solid line) due to the fact that the peak of the mean impedance profile is determined not only by the peak of the profiles in individual experiments but also by their slopes and amplitudes.

Figure 2: Ionic current contributing to membrane resonance properties of the PD neuron. **A.** The voltage response of the PD neuron to a ZAP current injection (as in Fig. 1) in control (Ctl) and after superfusion with Cs^+ to block I_h or Mn^{++} to block I_{Ca}. The vertical arrowhead in Ctl indicates the resonance frequency. The small horizontal dashed lines show the -60 mV level. **B.** The impedance profile of the PD neuron in control and after superfusion with Cs^+ (N = 4). Note the shift of f_{max} from 0.96 to 0.41 Hz. **C.** The impedance profile of the PD neuron in control and after superfusion with Mn^{++} (N = 4) which abolishes resonance. The shaded regions in B and C indicate one standard error.

Figure 3: I_h shapes the lower envelope of the voltage profile of the PD model neuron. All ionic currents other than I_{leak}, I_h, I_{Ca} and $I_{K(Ca)}$ have been removed **A.** The voltage response of the model PD neuron to a ZAP current injection in control (black) and after blocking I_h (red). The dashed curves mark the lower envelope of the voltage profiles (slightly displaced for clarity), indicating the effect of I_h in shaping the voltage response of the PD model

neuron. **B.** The voltage response (green) with the maximum conductance of I_h set to one half of the control value of 0.2 nS (black). **C.** The voltage response (orange) with the maximum conductance of I_h set to 0.3 nS (black). **D** The impedance profile of the traces shown in **A-C**. Note that increasing the maximum conductance of I_h shifts the resonance frequency to a slightly higher value. The small horizontal dashed line in A shows the -60 mV level in A-C.

Figure 4: I_h and I_{Ca}, respectively, shape the lower and upper envelope of the voltage profile of the PD model neuron. **A.** Same as Fig. 3A, showing the effect of blocking I_h (red) on the voltage response of the model neuron. Black trace is control. Dashed curves show the lower envelope of the voltage profile and the bars on the right indicate the voltage range at the highest frequency. **B.** A constant DC bias current (0.32 nA) was applied after blocking I_h to counteract the hyperpolarized voltage due to blocking I_h. Even with the depolarizing bias current, the effect of blocking I_h was mainly visible in shaping the lower envelope of the voltage profile (dashed curves). Note that the upper envelope still shows a local maximum. The bars on the right indicate the voltage range at the highest frequency. **C.** The voltage response of the model PD neuron after blocking I_{Ca} (green). Note the role of I_{Ca} in shaping of the upper envelope of the resonance envelope indicated with the dashed curves. **D.** Blocking both I_{Ca} and I_h (blue) removes the resonance property by reshaping both upper and lower envelopes (dashed curves) of the voltage profile. **E.** The impedance profile of the model PD neuron in control and the cases shown in **A-D**. Note when either the upper or lower envelopes of the voltage profile are reshaped, the resonance peak and f_{max} in the model neuron is abolished. The small horizontal dashed line in A shows the -60 mV level in A-D.

Figure 5: The effect of blocking potassium currents on the resonance profile. **A.** An example of the effect of TEA (which blocks both the delayed rectifier and calcium-dependent potassium currents) on the voltage response of the PD neuron to a ZAP current injection (amplitude ~1 nA) shows sporadic spikes at lower frequencies. **B.** When the conductance of the potassium currents is reduced to 20% of its original value in the computational model of the PD neuron (see Materials and Methods), in response to a ZAP

current injection it produces calcium spikes in a range of frequencies, similar to that observed in the biological neuron (panel A). C. Reducing the amplitude of the injected ZAP current in TEA, in some cases, enabled us to measure the impedance despite the presence of small spike-like responses in the voltage profile (C1; TEA panel). In these cases, when the TEA impedance was compared to control (C2) there was no large difference in the resonance frequency despite the larger impedance values, in TEA, at most frequencies. Dashed lines in A, B and C1 denote -50 mV.

Figure 6: The resonance frequency f_{max} of the PD neuron is correlated with its ongoing oscillation frequency $f_{pyloric}$. **A.** Negative or positive DC current injection in the PD neuron decreases or increases $f_{pyloric}$ (left). After superfusion with TTX to abolish activity, the voltage traces of the same PD neuron are shown (right) in response to the injection of a ZAP current plus the same bias current as the left column. The arrowhead shows the resonance frequency of the PD neuron. The small horizontal dashed lines show the -60 mV level. **B.** The f_{max} of the PD neuron plotted versus $f_{pyloric}$ when both values are changed by injection of the same DC bias currents. The dashed line shows the linear fit of the data points ($y = 0.315\ x + 0.835$, $R^2 = 0.77 \pm 0.12$, $p < 0.007$, N = 7 experiments, 2-4 data points per experiment).

Figure 7: Alteration of the oscillation frequency ($f_{pyloric}$) of the PD neuron by shifting its membrane resonance frequency f_{max} using the dynamic clamp technique. **A.** Adding or subtracting g_{Ca} shifts both f_{max} and $f_{pyloric}$. **A1.** Voltage traces of the PD neuron during ongoing oscillations in normal saline (upper traces) and in response to a ZAP current applied in TTX (lower traces). The left column (blue) shows the effect of subtracting a dynamic-clamp artificial I_{Ca} whereas the right column (red) shows the effect of adding I_{Ca} (see text). **A2.** Impedance profiles measured from traces in A1, shown as a function of frequency. **B.** Adding or subtracting g_h shifts both f_{max} and $f_{pyloric}$. **B1.** As in A1, the left column (blue) shows the effect of subtracting a dynamic-clamp artificial I_h whereas the right column (red) shows the effect of adding I_h (see text). **B2.** Impedance profiles measured from traces in B1, shown as a function of frequency. **C.** Normalized changes in $f_{pyloric}$ induced by changing either I_{Ca} or I_h are correlated to normalized changes in f_{max}

corresponding to the subtraction or addition of the same dynamic-clamp artificial currents. The dotted line indicates no change in f_{max}. The dashed line shows a linear fit of data points (R^2 = 0.57 ± 0.088, p = 0.001, N = 5 experiments; up to 6 negative and 6 positive conductance values were done in each experiment). The blue square shows the average change obtained by the subtraction of dynamic-clamp artificial currents ($\Delta f_{pyloric} / f_{pyloric}$ = -0.035 ± 0.016 and $\Delta f_{max} / f_{max}$ = -0.36 ± 0.072) and the red square shows the average obtained by the addition of dynamic-clamp artificial currents ($\Delta f_{pyloric} / f_{pyloric}$ = 0.081 ± 0.016 and $\Delta f_{max} / f_{max}$ = 0.581 ± 0.115) for both I_{Ca} and I_h.

TABLE

	g_{max}	E_{rev}	V_m	k_m	τ_{mhi}	τ_{mlo}	p	V_h	k_h	τ_{hhi}	τ_{hlo}	q
unit	nS	mV			ms			mV		ms		
$I_{Ca,dyn}$	5, -5	110	-30	-20	400	25	3	-	-	-	-	0
$I_{h,dyn}$	12, -12	-20	-50	6	250	50	1	-	-	-	-	0

Table 1. Parameters of dynamic clamp-injected currents. Note that the positive (negative) g_{max} values indicated were the maximum values used to shift the resonance peak to higher (lower) frequencies.

Fig. 1

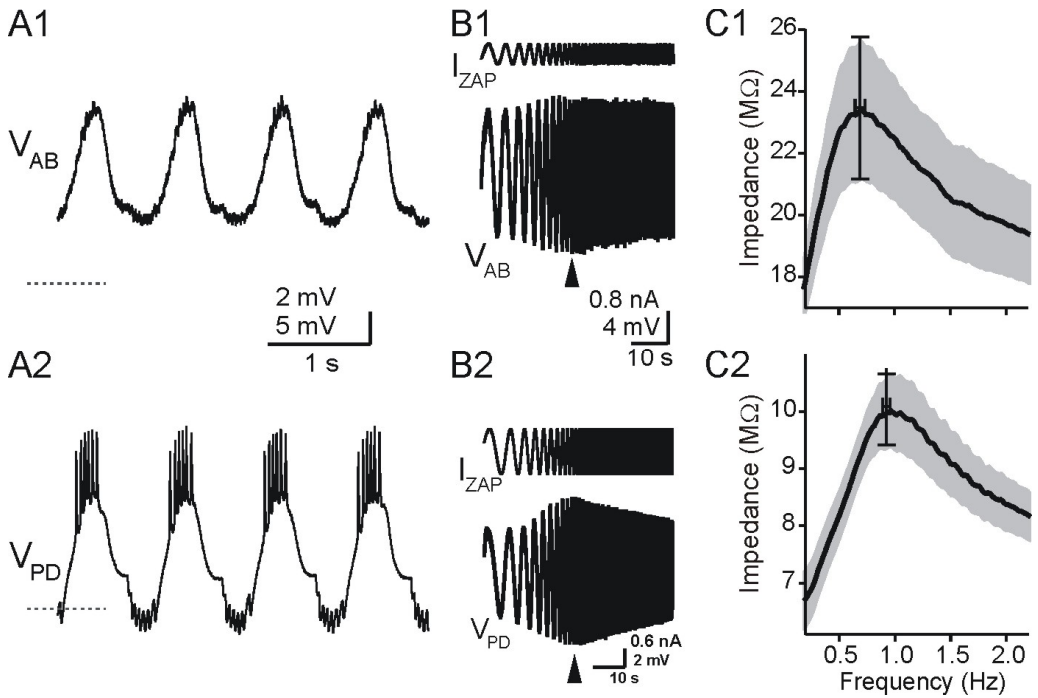
A1
V_{AB}
2 mV
5 mV
1 s
B1
I_{ZAP}
V_{AB}
0.8 nA
4 mV
10 s
C1
Impedance (MΩ)
26
24
22
20
18
A2
V_{PD}
B2
I_{ZAP}
V_{PD}
0.6 nA
2 mV
10 s
C2
Impedance (MΩ)
10
9
8
7
0.5 1.0 1.5 2.0
Frequency (Hz)

Fig. 2

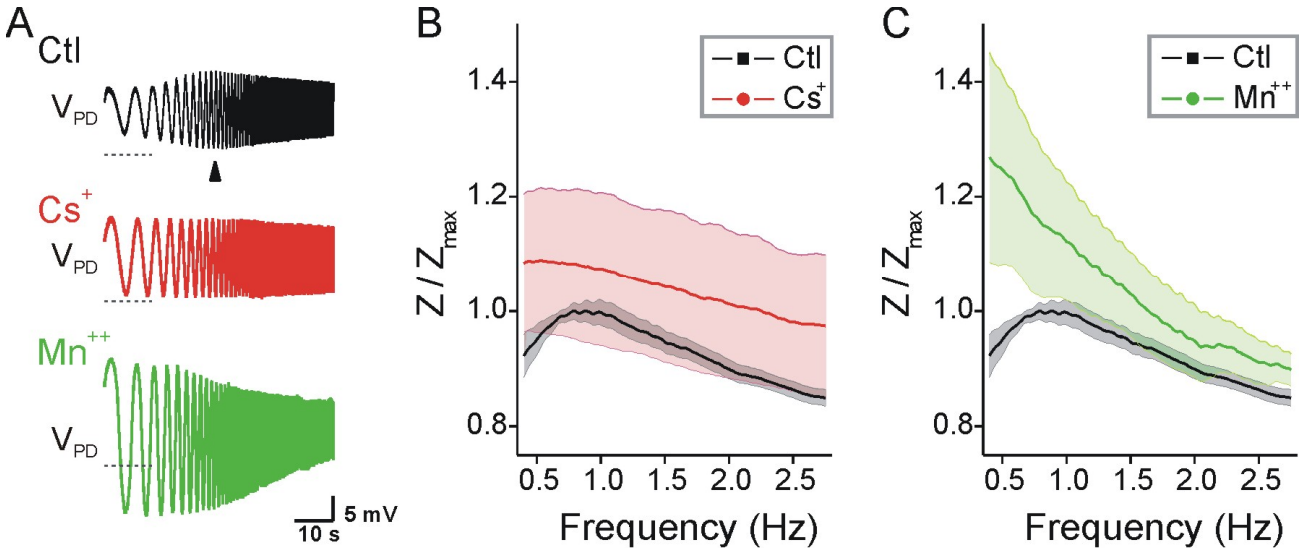
A
Ctl
V_{PD}
Cs^+
V_{PD}
Mn^{++}
V_{PD}
5 mV
10 s
B
Ctl
Cs^+
Z / Z_{max}
1.4
1.2
1.0
0.8
0.5 1.0 1.5 2.0 2.5
Frequency (Hz)
C
Ctl
Mn^{++}
Z / Z_{max}
1.4
1.2
1.0
0.8
0.5 1.0 1.5 2.0 2.5
Frequency (Hz)

Fig. 3

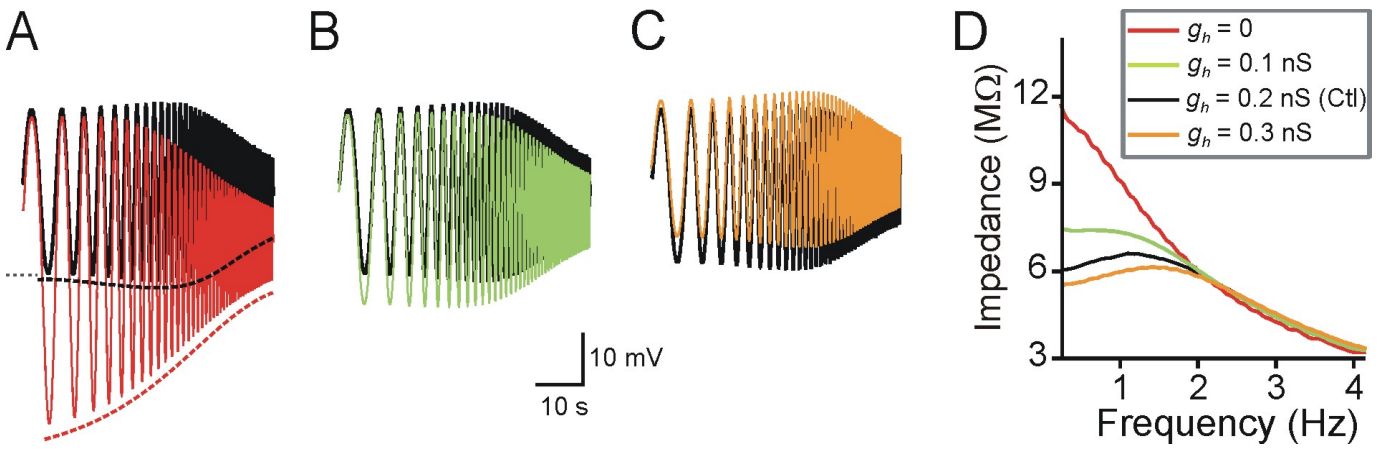
A
B
C
D
10 mV
10 s
Impedance (MΩ)
Frequency (Hz)
g_h = 0
g_h = 0.1 nS
g_h = 0.2 nS (Ctl)
g_h = 0.3 nS

Fig. 4

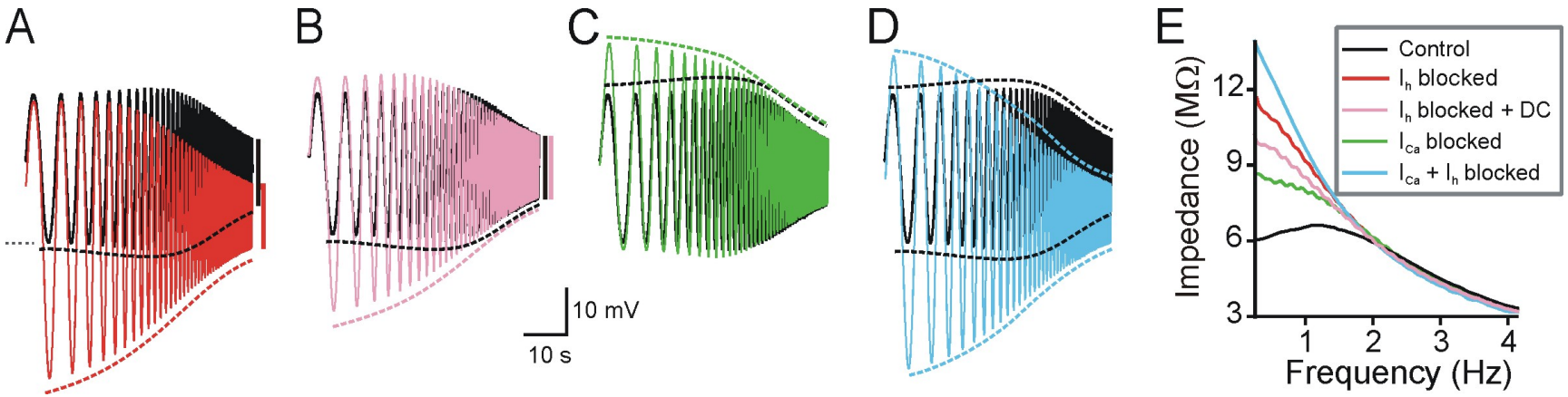
A
B
C
D
E
10 mV
10 s
Impedance (MΩ)
Frequency (Hz)
Control
I_h blocked
I_h blocked + DC
I_{Ca} blocked
I_{Ca} + I_h blocked

Fig. 5

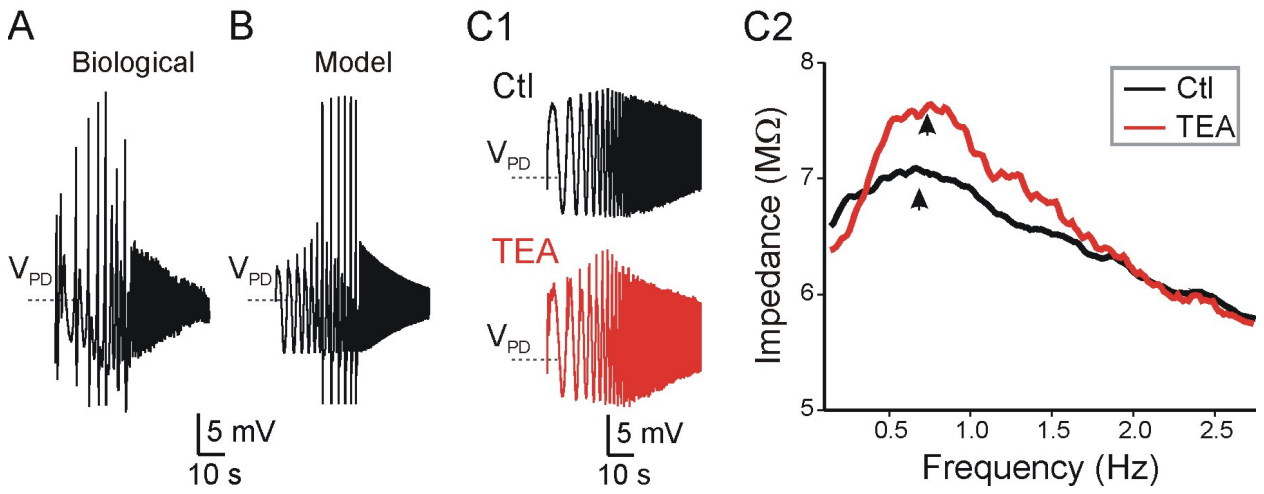
A
Biological
B
Model
C1
Ctl
TEA
V_{PD}
5 mV
10 s
C2
Ctl
TEA
Impedance (MΩ)
Frequency (Hz)

Fig. 6

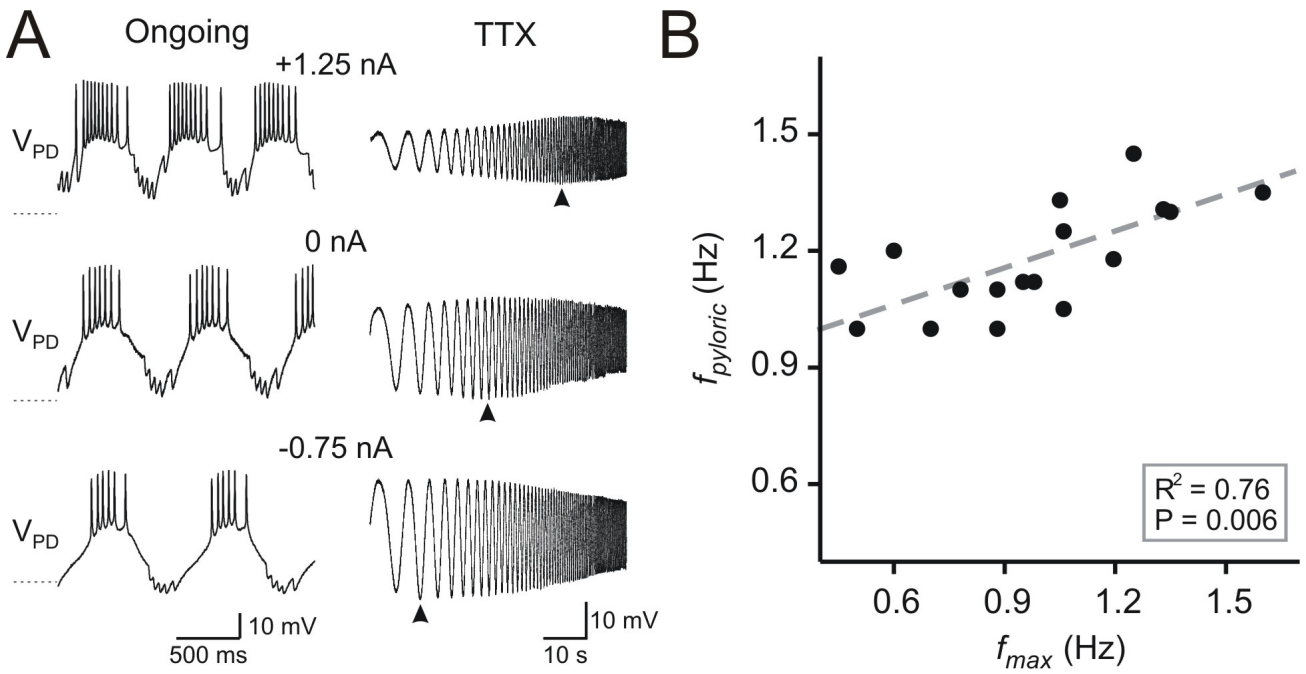
A
Ongoing
TTX
+1.25 nA
0 nA
-0.75 nA
V_{PD}
10 mV
500 ms
10 mV
10 s
B
$f_{pyloric}$ (Hz)
f_{max} (Hz)
R^2 = 0.76
P = 0.006

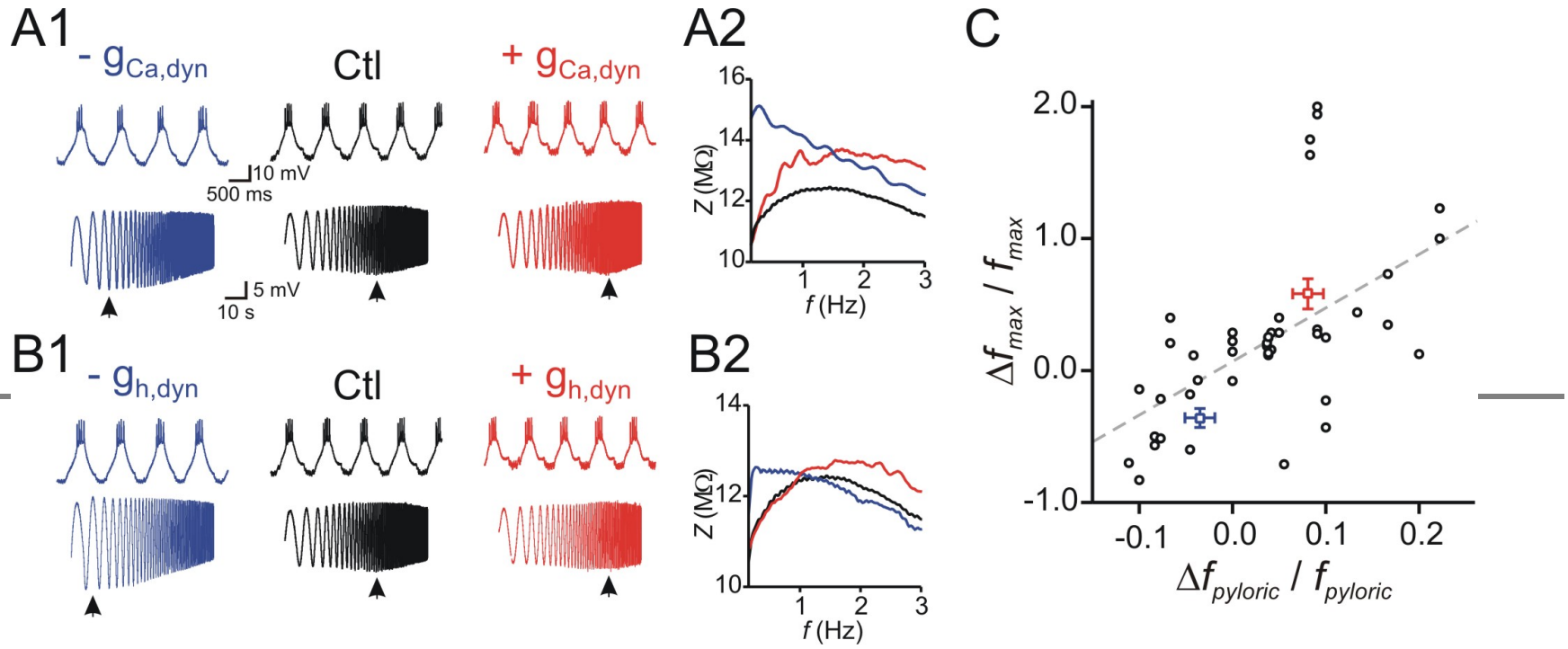
A1
- $g_{Ca,dyn}$
Ctl
+ $g_{Ca,dyn}$
10 mV
500 ms
5 mV
10 s
A2
Z (MΩ)
f (Hz)
B1
- $g_{h,dyn}$
Ctl
+ $g_{h,dyn}$
B2
Z (MΩ)
f (Hz)
C
$\Delta f_{max} / f_{max}$
$\Delta f_{pyloric} / f_{pyloric}$

Fig. 7